Merger estimates for rotating Kerr black holes in modified gravity

Shao-Wen Wei* and Yu-Xiao Liu†

Research Center of Gravitation, Lanzhou University, Lanzhou 730000, China,
Institute of Theoretical Physics, Lanzhou University, Lanzhou 730000, China
and Key Laboratory for Magnetism and Magnetic of the Ministry of Education,
Lanzhou University, Lanzhou 730000, China

(Received 25 April 2018; published 25 July 2018)

In this paper, we explore the signatures of nonrotating and rotating black hole mergers in the matter-free modified gravity. First, we solve the unstable circular null orbits and the innermost stable circular timelike orbits via the geodesic motion. The characteristic quantities of these orbits are systematically analyzed by varying the black hole spin and the scalar field parameter of the gravity. Then based on it, we study the ringdown modes from the light ring/quasinormal modes correspondence. The final spins of the merged black holes are also estimated with the Buonanno-Kidder-Lehner recipe. Several black hole merging cases are investigated in detail. All these results show that the black hole mergers are closely dependent on the scalar field parameter of the gravity.

DOI: 10.1103/PhysRevD.98.024042

I. INTRODUCTION

Recently, gravitational waves have been directly observed by LIGO and Virgo [1], and have opened a new window to probe the fundamental questions of our Universe and gravitational theory. As expected, these gravitational waves were produced by merging binary black holes or neutron stars. Particularly, the exact determination of the masses, spins, and other parameters for the initial and final black holes will greatly improve our test near the strong gravitational regimes. Moreover, different modified gravities are also expected to be tested or restricted by using the gravitational wave observations [2,3].

Although recent observations incline to support general relativity (GR) [4,5], some subtle potential deviations may be witnessed in the coming years when more merging events are detected and a higher improved signal-to-noise ratio is achieved. In order to discriminate different relevant gravity theories by the observations, one needs first to examine their differences. Importantly, it is necessary to identify the key signatures of the waveforms of the black hole mergers for these theories, which is also very useful to exactly determine the dynamic properties and the nature of these initial and final black holes.

On the other hand, there is an interesting modified gravity (MOG), the scalar-tensor-vector gravity theory proposed by Moffat [6]. Besides the metric tensor fields, extra massive vector field and scalar fields were introduced. The scalar fields strengthen the gravitational attraction, while the vector field produces an effective repulsive gravitational force. Such theory can be treated as an alternative to GR for dealing with the galaxy rotation curves and galaxy clusters without introducing the dark matter [7–9].

Particularly, many recent works were devoted to explore the novel properties of the nonrotating and rotating MOG black holes [10]. A black hole shadow was briefly examined in Ref. [11]. The thermodynamics of these black holes were studied in Ref. [12]. The geodesics and accretion disk were investigated in Refs. [13–17]. Misaligned spin merging black holes were discussed in Ref. [18]. And the quasinormal modes (QNMs) were calculated in Ref. [19]. All these results imply that there exists a significant difference between MOG and GR.

In the present work, we would like to consider the Kerr-MOG black hole merger, and two issues of the merger are studied. The first one is the gravitational wave emission patterns at the last stage, i.e., the ringdown stage, of the merger. In the eikonal limit, the QNMs are associated with the unstable circular null geodesics, the light ring, of the black hole in the asymptotically flat spacetime (for recent progress, see Refs. [20–22]). Although there exists a small deviation between the numerical data [23–26], it is still a good approximation. According to this light ring/QNM correspondence, the real part of the QNM is related to the angular velocity of the massless particle orbiting around the light ring. And its imaginary part is related to the Lyapunov exponent of the light ring. So through studying the light ring from the null geodesics, we can obtain the ringdown modes of the black hole merger. This has a theoretical guidance to distinguish this MOG from GR by probing the merger dynamics at the ringdown stage.

*weishw@lzu.edu.cn
†liuyx@lzu.edu.cn

Another issue of the merger we will pursue is the estimate of the final black hole spin. For this section, we adopt the Buonanno-Kidder-Lehner (BKL) recipe [27], which is based on the angular momentum and mass conservations. And such a recipe has gained great success on estimating the final black hole spin. Moreover, this approach has two advantages. First, it considers the orbital angular momenta and both initial spins of the merged black holes. Second, it can be applied to general mass ratio mergers. Then through solving the innermost stable circular orbits (ISCO) from the timelike geodesics, one can obtain the final spin of the black hole following this BKL recipe. The study has been carried out for the Kerr black hole and Einstein-Maxwell-dilaton black hole mergers. Comparing with the numerical simulations, the result shows that the BKL formula is quite accurate [27,28]. More importantly, such an approach can also be easily generalized to other different merger configurations, and some interesting and novel dynamics might be explored immediately. For example, the "flip" phenomenon was discussed with such a recipe. Moreover, it was found that it is impossible to spin up a black hole to extremal values through merger scenarios [27]. However, considering the energy loss, a near extreme spinning black hole can be produced by equal mass maximally spinning aligned mergers [29].

This paper is organized as follows. In Sec. II, we give a brief review of the black hole metric and its geodesics. Based on the geodesics, we calculate the radius and minimum impact parameter for the light rings. Further, we study the QNMs at the ringdown stage in Sec. III. In Sec. IV, we first numerically calculate the ISCO. Then based on the result, we follow the BKL recipe and estimate the final black hole spins for several merger configurations. Finally, the conclusions are presented in Sec. V.

II. KERR-MOG BLACK HOLE AND GEODESICS

The action of the scalar-tensor-vector gravity is formulated as [6]

$$S = S_{\rm GR} + S_\phi + S_S + S_M, \tag{1}$$

with

$$S_{\rm GR} = \frac{1}{16\pi}\int d^4x\sqrt{-g}\frac{R}{G}, \tag{2}$$

$$S_\phi = \int d^4x\sqrt{-g}\left(-\frac{1}{4}B^{\mu\nu}B_{\mu\nu} + \frac{1}{2}\mu^2\phi^\mu\phi_\mu\right), \tag{3}$$

$$S_S = \int d^4x\sqrt{-g}\frac{1}{G^3}\left(\frac{1}{2}g^{\mu\nu}\nabla_\mu G\nabla_\nu G - V(G)\right) + \int d^4x\frac{1}{\mu^2 G}\left(\frac{1}{2}g^{\mu\nu}\nabla_\mu\mu\nabla_\nu\mu - V(\mu)\right), \tag{4}$$

where ϕ^μ is a Proca type massive vector field with mass μ, $G(x)$ and $\mu(x)$ are two scalar fields, and their potentials are, respectively, $V(G)$ and $V(\mu)$. S_M denotes the matter action. The tensor field $B_{\mu\nu} = \partial_\mu\phi_\nu - \partial_\nu\phi_\mu$, and it satisfies the following equations:

$$\nabla_\nu B^{\mu\nu} = 0, \tag{5}$$

$$\nabla_\sigma B_{\mu\nu} + \nabla_\mu B_{\nu\sigma} + \nabla_\nu B_{\sigma\mu} = 0. \tag{6}$$

The energy momentum tensor for the vector field is

$$T_{\phi\mu\nu} = -\frac{1}{4\pi}\left(B_\mu^\sigma B_{\nu\sigma} - \frac{1}{4}g_{\mu\nu}B^{\sigma\beta}B_{\sigma\beta}\right). \tag{7}$$

Since the effect of the mass μ of the vector field displays at kiloparsec scales from the source, it can be neglected for a black hole solution. Moreover, we can also treat G as a constant independent of the spacetime coordinates. With this hypothesis, the action will be simplified and easy to deal with,

$$S = \int d^4x\sqrt{-g}\left(\frac{R}{16\pi G} - \frac{1}{4}B^{\mu\nu}B_{\mu\nu}\right). \tag{8}$$

The corresponding field equation reads

$$G_{\mu\nu} = -8\pi G T_{\phi\mu\nu}, \tag{9}$$

and G corresponds to Newton's gravitational constant as $G = G_N(1+\alpha)$ with α being a dimensionless parameter. So α can be used to measure the deviation of MOG from GR.

The rotating Kerr-MOG black hole solution can be obtained by solving the field equation (9). In Boyer-Lindquist coordinates, the metric is given by [10]

$$ds^2 = -\frac{\Delta}{\rho^2}(dt - a\sin^2\theta d\phi)^2 + \frac{\rho^2}{\Delta}dr^2 + \rho^2 d\theta^2 + \frac{\sin^2\theta}{\rho^2}(adt - (r^2+a^2)d\phi)^2, \tag{10}$$

with the metric functions given by

$$\Delta = r^2 - 2G_N(1+\alpha)mr + a^2 + m^2G_N^2\alpha(1+\alpha), \tag{11}$$

$$\rho^2 = r^2 + a^2\cos^2\theta. \tag{12}$$

For simplicity, we adopt $G_N = 1$. The parameter m is related to the Arnowitt-Dese-Misner mass M of the black hole as [17]

$$M = (1+\alpha)m. \tag{13}$$

Solving $\Delta = 0$, we can obtain the radius of the black hole horizon

$$r_{\pm} = M \pm \sqrt{\frac{M^2}{1+\alpha} - a^2}. \tag{14}$$

It is clear that such a black hole can possess two horizons for $M^2 > (1+\alpha)a^2$, one degenerate horizon for $M^2 = (1+\alpha)a^2$, and no horizon related to naked singularity for $M^2 < (1+\alpha)a^2$. So the black hole has a maximum spin

$$\frac{a_{\max}}{M} = \frac{1}{\sqrt{1+\alpha}}. \tag{15}$$

It is worth noting that this Kerr-MOG black hole will reduce to the Kerr black hole when $\alpha = 0$. On the other hand, if we set $a = 0$, it will be a static black hole with two horizons $r_{\pm} = M(1 \pm 1/\sqrt{1+\alpha})$. Further taking $\alpha = 0$, the Schwarzschild black hole solution will be recovered.

In this rotating Kerr-MOG background, the geodesics of a test particle with unit mass is [10]

$$\dot{t} = \frac{g_{\phi\phi}E + g_{\phi t}L}{g_{\phi t}^2 - g_{tt}g_{\phi\phi}}, \tag{16}$$

$$\dot{\phi} = -\frac{g_{tt}L + g_{t\phi}E}{g_{t\phi}^2 - g_{tt}g_{\phi\phi}}, \tag{17}$$

$$\rho^2\dot{r} = \sigma_r\sqrt{\mathcal{R}}, \tag{18}$$

$$\rho^2\dot{\theta} = \sigma_\theta\sqrt{\Theta}, \tag{19}$$

where

$$\mathcal{R} = (aL - E(r^2+a^2))^2 - \left(a^2 + r^2 - 2Mr + \frac{\alpha M^2}{1+\alpha}\right) \times (\mathcal{K} + \mu^2 r^2), \tag{20}$$

$$\Theta = \mathcal{K} - a^2\mu^2\cos^2\theta - (aE\sin^2\theta - L)^2\csc^2\theta. \tag{21}$$

The sign functions $\sigma_r = \pm$ and $\sigma_\theta = \pm$ are independent from each other. And $\mathcal{K}$ is the Carter constant. The values of μ^2 are 1 and 0 for massive particle and photon, respectively. Here, we consider the motion limited in the equatorial plane. So we have $\theta = \frac{\pi}{2}$ and $\mathcal{K} = (aE - L)^2$. Then we can reexpress Eq. (18) as the following form:

$$\dot{r}^2 + V_{\text{eff}} = 0, \tag{22}$$

where the effective potential is given by

$$V_{\text{eff}} = -\frac{\mathcal{R}}{\rho^4}. \tag{23}$$

III. RINGDOWN MODES

The final stage of a black hole merger is known as the ringdown stage. In this stage, the final black hole settles to a stationary one, and it is characterized by linearized vibrational modes, i.e., the QNMs. In the eikonal limit, such a mode is associated with the spacetime's light ring. And this light ring/QNM correspondence is effective for an asymptotically flat spacetime. The modes of $n = |m|$ are considered to be the most powerful emitters during the gravitational waves and thus are most easily detectable by observatories, so we mainly focus on them in this paper. Fortunately, these modes are also the easiest ones to fit the eikonal approximation. More interestingly, these modes with positive or negative m are related with the equatorial prograde or retrograde orbital motion.

These modes are expressed in the following form [20,30–32]:

$$\omega_{\text{QNM}} = \Omega_c m - i(n + 1/2)|\lambda|, \tag{24}$$

where m, n, Ω_c, and λ are the quantum overtone number, angular momentum, angular velocity, and Lyapunov exponent of the light ring, respectively. Moreover, λ and Ω_c can be calculated with the geodesics

$$\lambda = \sqrt{-\frac{V''_{\text{eff}}}{2\dot{t}^2}}\bigg|_{r_c}, \qquad \Omega_c = \frac{\dot{\phi}}{\dot{t}}\bigg|_{r_c}, \tag{25}$$

with r_c being the radius of the light ring. Here the effective potential for the photon reads

$$V_{\text{eff}} = \frac{(aE - L)^2\Delta - (aL - E(a^2+r^2))^2}{\rho^4}. \tag{26}$$

The characteristic parameters of the light rings are determined by the conditions

$$V_{\text{eff}} = 0, \qquad V'_{\text{eff}} = 0, \qquad V''_{\text{eff}} < 0. \tag{27}$$

Substituting the effective potential into these conditions, one will get

$$(aL - E(a^2+r^2))^2 - (aE - L)^2\Delta = 0, \tag{28}$$

$$4Er(aL - E(a^2+r^2)) - (aE - L)^2\Delta' = 0, \tag{29}$$

$$8E^2r^2 - 4E(aL - E(a^2+r^2)) - (aE - L)^2\Delta'' > 0. \tag{30}$$

Solving them, we can obtain the radius r_c and the minimum impact parameter u_c of the light rings. For the nonrotating black hole with $a = 0$, we have

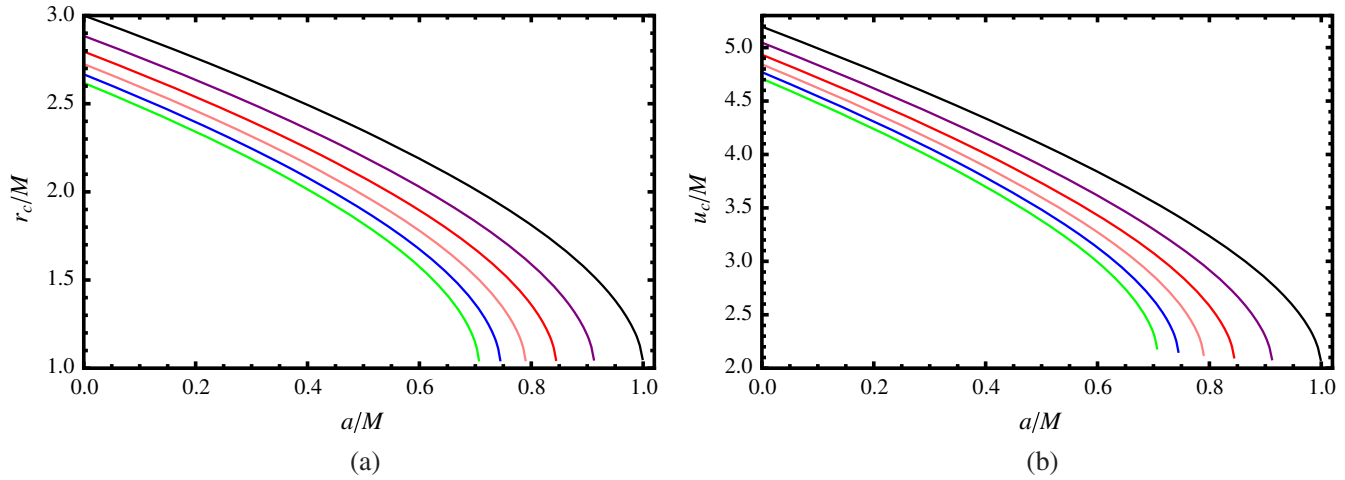

FIG. 1. Radius and minimum impact parameter for the prograde light rings. (a) r_c vs a. (b) u_c vs a. The parameter $\alpha = 0$, 0.2, 0.4, 0.6, 0.8, 1 from top to bottom.

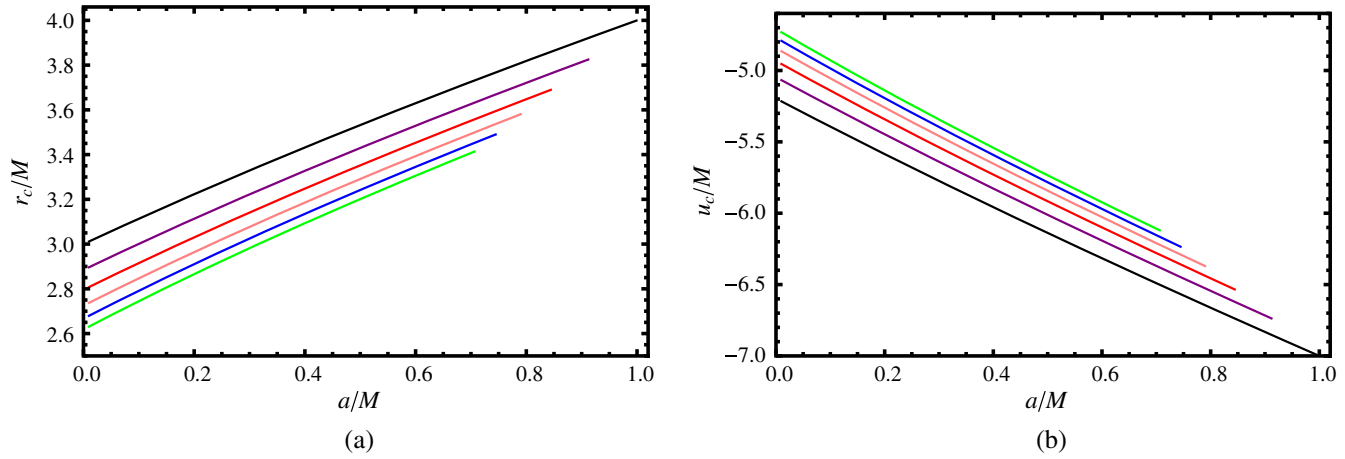

FIG. 2. Radius and minimum impact parameter for the retrograde light rings. (a) r_c vs a with $\alpha = 0$, 0.2, 0.4, 0.6, 0.8, 1 from top to bottom. (b) u_c vs a with $\alpha = 0$, 0.2, 0.4, 0.6, 0.8, 1 from bottom to top.

$$\frac{u_c}{M} = \frac{L}{ME} = \frac{\sqrt{27+45\alpha+17\alpha^2-\alpha^3+((1+\alpha)(9+\alpha))^{3/2}}}{\sqrt{2}(1+\alpha)}, \tag{31}$$

$$\frac{r_c}{M} = \frac{3+3\alpha+\sqrt{(1+\alpha)(9+\alpha)}}{2(1+\alpha)}. \tag{32}$$

When $\alpha = 0$, the above result reduces to the Schwarzschild black hole case, i.e.,

$$\frac{u_c}{M} = 3\sqrt{3}, \qquad \frac{r_c}{M} = 3. \tag{33}$$

On the other hand, for the rotating black hole with $a \neq 0$, due to the dragging effect, the light rings will be different for prograde and retrograde cases. Although it is impossible to obtain the analytical formula, we can numerically solve these conditions (27). And the results are presented in Figs. 1 and 2 for the prograde and retrograde orbits. For the prograde orbit, we find that both r_c and u_c decrease with the spin a and the parameter α. For the retrograde orbit, r_c increases with the spin a and decreases with α, while u_c decreases with a and increases with α.

For the nonrotating black hole, the angular velocity and Lyapunov exponent of the unstable null geodesics are analytically obtained

$$\Omega_c M = \frac{\sqrt{2}(1+\alpha)}{\sqrt{27+45\alpha+17\alpha^2-\alpha^3+((1+\alpha)(9+\alpha))^{3/2}}}, \tag{34}$$

$$\lambda M = \frac{2\sqrt{(1+\alpha)^3(9+\alpha+\sqrt{9+10\alpha+\alpha^2})}}{(3+3\alpha+\sqrt{9+10\alpha+\alpha^2})^2}. \tag{35}$$

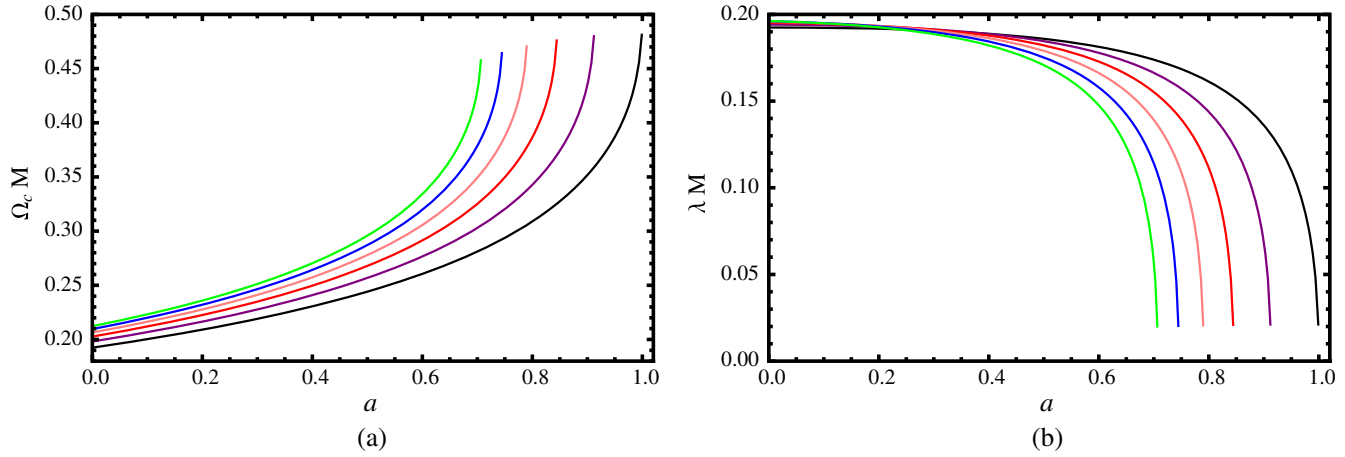

FIG. 3. Angular velocity and Lyapunov exponent for the prograde light rings. (a) Ω_c vs a. (b) λ vs a. The parameter $\alpha = 0$, 0.2, 0.4, 0.6, 0.8, 1 from right to left.

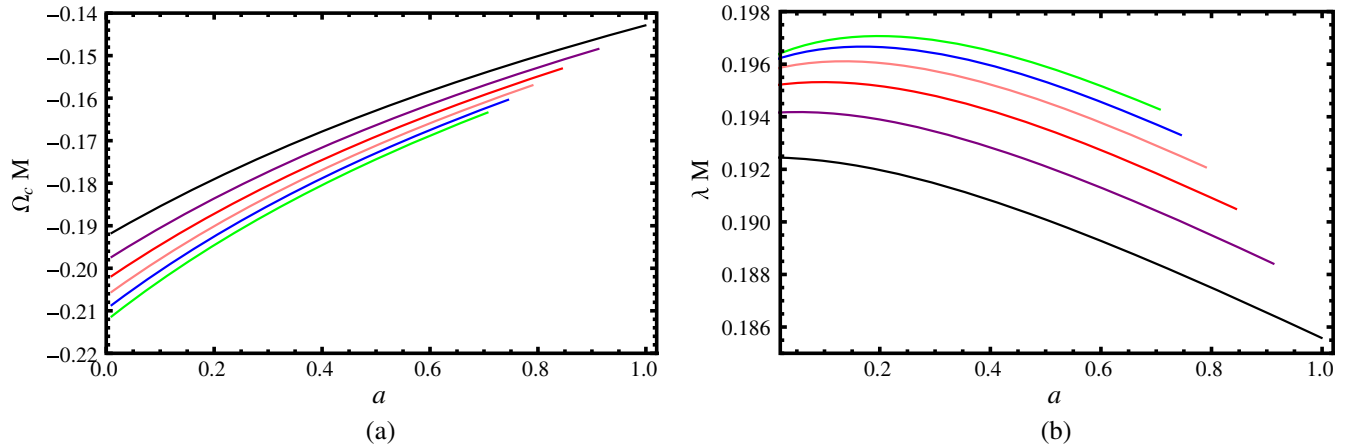

FIG. 4. Angular velocity and Lyapunov exponent for the retrograde light rings. (a) Ω_c vs a with parameter $\alpha = 0$, 0.2, 0.4, 0.6, 0.8, 1 from top to bottom. (b) λ vs a with parameter $\alpha = 0$, 0.2, 0.4, 0.6, 0.8, 1 from bottom to top.

For the rotating black hole, the results are shown in Figs. 3 and 4. For the prograde orbit, with the increase of spin a, the angular velocity Ω_c increases, while the Lyapunov exponent λ decreases. Moreover, Ω_c increases with α. The Lyapunov exponent λ increases with α for small a, and decreases with α for large a. For the retrograde orbit, Ω_c increases with spin a and decreases with α. On the other hand, the Lyapunov exponent λ increases with α. And for small fixed α, λ slightly decreases with the spin a. However, for large fixed α, λ first increases and then decreases with a.

Before ending this section, we would like to give some notes for the light ring/QNM correspondence. First, our calculation is mainly based on the geodesics, which measures the motion of a pointlike test particle in the background. So it may be in good approximation if one of the black holes is small and the other one is huge during the merger. Interestingly, the results given in Refs. [33–35] imply that the point particle approximation is also accurate for the equal mass black hole collisions. Thus such correspondence is reasonable for calculating the ringdown modes during the black hole merger.

On the other hand, it is worthwhile to examine the influence of the additional field, i.e., the scalar field parameter α, on the light ring/QNM correspondence. As shown in Refs. [25,26], the QNMs for the black hole in the Einstein-dilaton-Gauss-Bonnet gravity have a close relation with the coupling parameter. It is also foundd that the geodesics correspondence predicts only the axial modes of the perturbation. And they are consistent with each other for a small coupling parameter. Here let us turn to consider the influence of the parameter α on the light ring/QNM correspondence. For simplicity, we only consider the nonrotating case. Here we list the numerical data in Table I for the QNMs calculated from the asymptotic iteration method [19] and from Eqs. (34) and (35). From the table, we can see that the real part and the imaginary part of the QNMs have different behaviors with the parameter α. For $\alpha = 0$, the real parts of the QNMs obtained from the

TABLE I. QNMs for the nonrotating black hole in modified gravity. The first row shows the QNMs for the electromagnetic perturbation with $n = |m| = 3$ obtained with the asymptotic iteration method given in Ref. [19]. The second row is obtained with Eqs. (34) and (35). The parameter δ measures the relative deviation between these two methods.

	$\alpha = 0$	$\alpha = 1$	$\alpha = 4$	$\alpha = 9$
AIM [19]	0.5779 − 0.7063i	0.6891 − 0.7200i	0.7687 − 0.6988i	0.7927 − 0.6743i
Light ring/QNM	0.5774 − 0.6736i	0.6370 − 0.6868i	0.6922 − 0.6753i	0.7177 − 0.6582i
δ [%]	0.09 − 4.63i	7.56 − 4.61i	9.95 − 3.36i	9.46 − 2.39i

two methods highly coincide with each other, and the relative deviation $\delta = 0.09\%$. Moreover, the δ of the real part will increase with α. For example, δ approaches about 10% for $\alpha = 9$. In contrast, the relative deviation of the imaginary part of the QNMs has a slight decrease with α, and it is always under 5% for $\alpha = 0$–9. Combining with the result of the real part and the imaginary part of the QNM, we can arrive at the conclusion that the light ring/QNM correspondence is effective for the small parameter α. Hence, we only limit our attention to the small parameter, i.e., $\alpha \leq 1$.

IV. FINAL SPIN ESTIMATION

A. BKL recipe

Here we would like to briefly review the BKL recipe, which mainly depends on the conservations and is very easily understood. First, it considers that the mass of this merged system is conserved. Therefore, the mass of the final black hole equals the total mass of the initial black holes, i.e.,

$$M = M_1 + M_2. \tag{36}$$

To the first order, this is a good approximation. For example, the total radiated energy remains very small, about $M_{\text{radiated}} \sim 5\% M_{\text{initial}}$, in the gravitational wave observations [1].

On the other hand, for a reasonable merger, the two black holes orbit around each other during the first stage, i.e., the inspiral stage. Due to the energy loss via a gravitational wave emission, the binary orbit contracts gradually and the system evolves quasiadiabatically. During this stage, one can assume that the individual spins of the black holes will remain constant. Once the ISCO radius is reached, the orbit becomes unstable. This will lead to a merger, and then a final black hole is formed. At this stage, the radiation of the angular momentum with respect to that of the system is small. So the angular momentum of the system can be treated as a conserved quantity. Moreover, it is justified to estimate the contribution of the orbital angular momentum to the final black hole spin by adopting the orbital angular momentum of a test particle orbiting at the ISCO of the final black hole. Finally, the dimensionless final black hole spin a_f can be expressed as [27]

$$a_f = \frac{\tilde{L}_{\text{orb}}(r_{\text{ISCO}}, a_f)}{M} + \frac{M_1 a_1}{M} + \frac{M_2 a_2}{M}, \tag{37}$$

where $\tilde{L}_{\text{orb}}(r_{\text{ISCO}}, a_f)$ denotes the orbital angular momentum of a test particle with reduced mass $M_1 M_2/M$ orbiting at the ISCO of the final black hole with spin a_f. Without loss of generality, we can assume $M_1 \geq M_2$, and then the final spin can also be reexpressed in the following convenient form [27]:

$$a_f = L(r_{\text{ISCO}}, a_f)\nu + \frac{\chi_1 M}{4}\left(1 + \sqrt{1 - 4\nu}\right)^2 + \frac{\chi_2 M}{4}\left(1 - \sqrt{1 - 4\nu}\right)^2, \tag{38}$$

where $\chi_i = a_i/M_i$ is the dimensionless spins of the initial black holes and $L(r_{\text{ISCO}}, a_f)$ is the angular momentum of a unit mass test particle. The mass parameter $\nu = \frac{M_1 M_2}{M^2}$ and has a value in the range of $[0, 1/4]$. By solving the timelike geodesics, we can obtain the radius and the orbital angular momentum of the ISCO. Then given the initial mass parameter ν and spins χ_1 and χ_2, the final black hole spin can be calculated with Eq. (38). Importantly, since the parameter α deforms the gravitational constant characterized by the spacetime background, we fix α before and after the black hole merger.

B. ISCO

As mentioned above, in order to obtain the final spin of the black hole, we first need to solve the ISCO. So here we will consider such a special orbit for a test particle. From the geodesics, the conditions to determine the ISCO are

$$V_{\text{eff}} = 0, \qquad \partial_r V_{\text{eff}} = 0, \qquad \partial_{r,r} V_{\text{eff}} = 0. \tag{39}$$

Plunging the effective potential, the conditions reduce to

$$(aL - E(a^2 + r^2))^2 - ((aE - L)^2 + \mu^2 r^2)\Delta = 0, \tag{40}$$

$$4Er(aL - E(a^2 + r^2)) + 2\mu^2 r\Delta + ((aE - L)^2 + \mu^2 r^2)\Delta' = 0, \tag{41}$$

$$4E(aL - E(a^2 + r^2)) - 8E^2 r^2 + 2\mu^2\Delta + 4\mu^2 r\Delta' + ((aE - L)^2 + \mu^2 r^2)\Delta'' = 0. \tag{42}$$

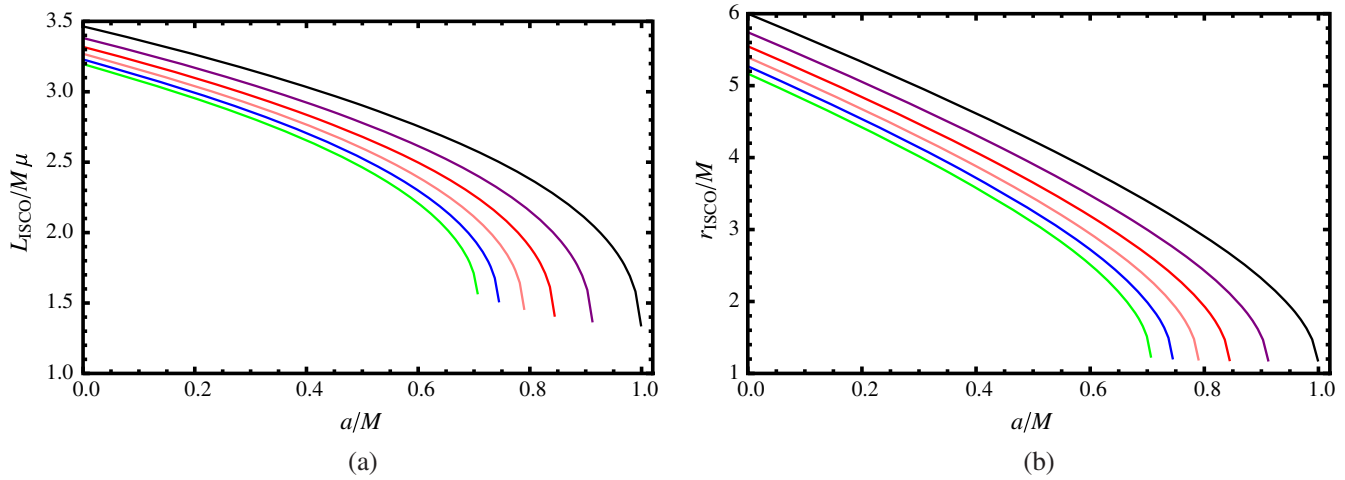

FIG. 5. Angular momentum and radius for the prograde ISCO. (a) $L_{\rm ISCO}$ vs a. (b) $r_{\rm ISCO}$ vs a. Parameter $\alpha = 0, 0.2, 0.4, 0.6, 0.8, 1$ from top to bottom.

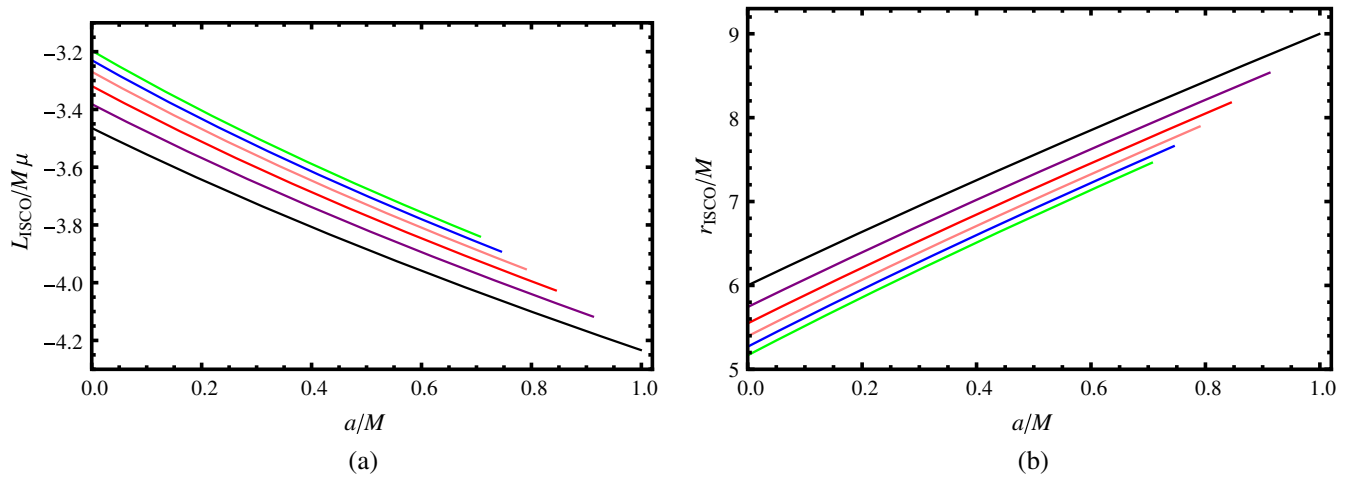

FIG. 6. Angular momentum and radius for the retrograde ISCO. (a) $L_{\rm ISCO}$ vs a with $\alpha = 0, 0.2, 0.4, 0.6, 0.8, 1$ from bottom to top. (b) $r_{\rm ISCO}$ vs a with $\alpha = 0, 0.2, 0.4, 0.6, 0.8, 1$ from top to bottom.

For the nonrotating black hole, we can express the angular momentum and energy in terms of the radius of the ISCO as

$$L/\mu = \pm\frac{r\sqrt{M(r - M\alpha + r\alpha)}}{2M^2\alpha - 3Mr(1+\alpha) + r^2(1+\alpha)}, \quad (43)$$

$$E/\mu = \frac{M^2\alpha - 2Mr(1+\alpha) + r^2(1+\alpha)}{r\sqrt{(1+\alpha)(2M^2\alpha - 3Mr(1+\alpha) + r^2(1+\alpha))}}. \quad (44)$$

And the radius of the ISCO is given by

$$r_{\rm ISCO}/M = 2 + (1+\alpha)^{-\frac{2}{3}}K^{\frac{1}{3}} + (4+\alpha)(1+\alpha)^{-\frac{1}{3}}K^{-\frac{1}{3}}, \quad (45)$$

where $K = 8 + \alpha^2 + (7 + \sqrt{5+\alpha})\alpha$. When $\alpha = 0$, one will get

$$r_{\rm ISCO}/M = 6, \qquad L_{\rm ISCO}/M\mu = 2\sqrt{3},$$
$$E_{\rm ISCO}/\mu = \frac{2\sqrt{2}}{3}, \quad (46)$$

for the Schwarzschild black hole. On the other hand, when $a \neq 0$, the analytical result can be obtained for the Kerr black hole with $\alpha = 0$; see Ref. [36]. When $\alpha \neq 0$, no analytical result is available. Nevertheless, we can numerically solve Eq. (39). The results are listed in Figs. 5 and 6 for prograde and retrograde ISCOs, respectively. For the prograde ISCO, both the angular momentum $L_{\rm ISCO}$ and radius $r_{\rm ISCO}$ decrease with the black hole spin a and the parameter α. For the retrograde ISCO, we clearly see that the angular momentum $L_{\rm ISCO}$ decreases and the radius $r_{\rm ISCO}$ increases with the spin a. However, $L_{\rm ISCO}$ increases and $r_{\rm ISCO}$ decreases with α.

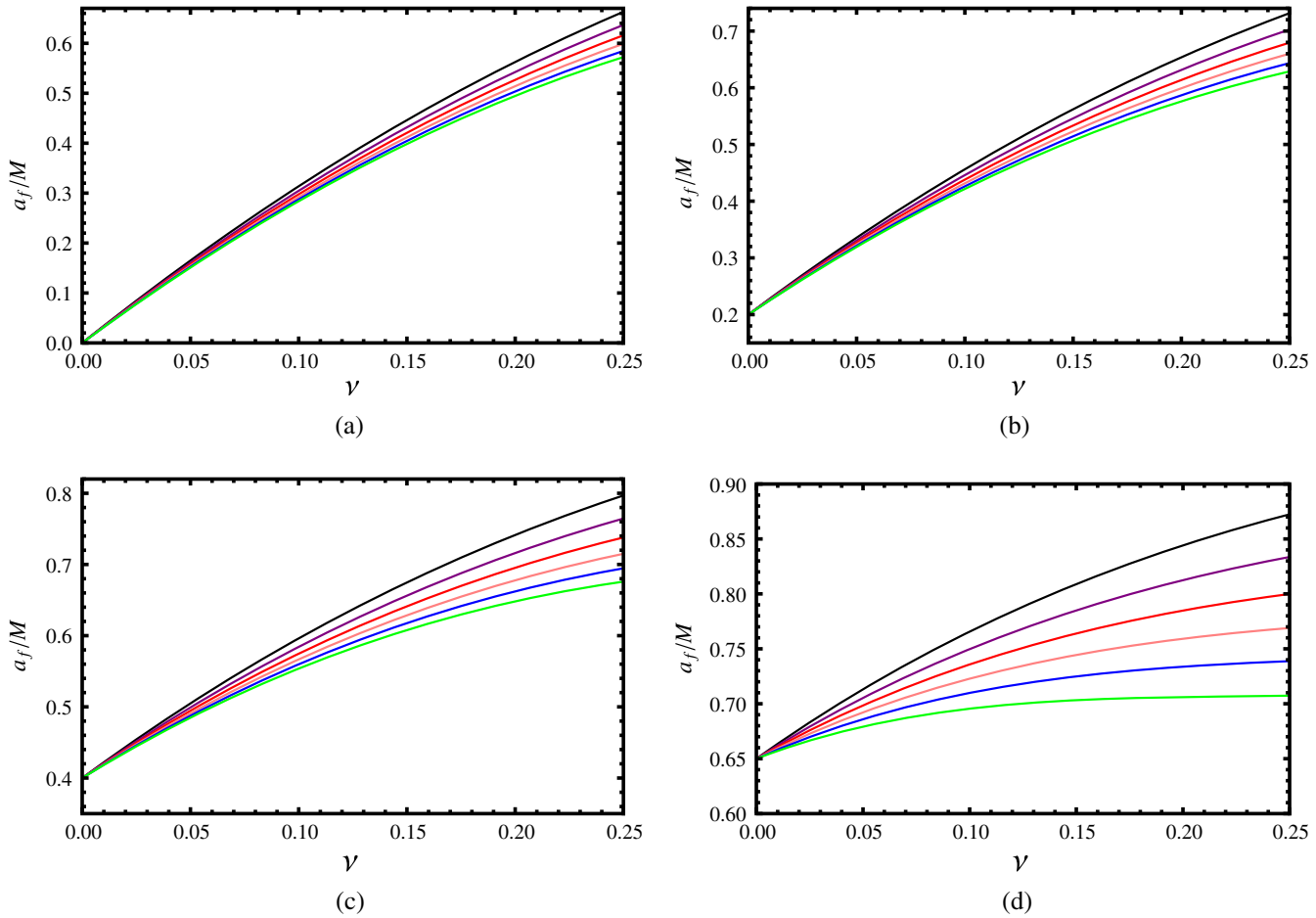

FIG. 7. Final spin a_f vs mass parameter ν for equal spin merger. (a) $\chi = 0$. (b) $\chi = 0.2$. (c) $\chi = 0.4$. (d) $\chi = 0.65$. The parameter $\alpha = 0$, 0.2, 0.4, 0.6, 0.8, 1 from top to bottom.

C. Equal spin merger

Based on the study of the ISCO for the black hole, we would like to estimate the final spin parameter of the merger. First, we consider a simple case where the two black holes have equal spin, i.e., $\chi_1 = \chi_2 = \chi$. Therefore, the final spin (38) will be of the form

$$a_f = L(r_{\rm ISCO}, a_f)\nu + M(1-2\nu)\chi. \tag{47}$$

Given ν and χ, we can solve the final spin from the above equation. Here we plot the final spin a_f as a function of the mass parameter ν for $\chi = 0$, 0.2, 0.4, and 0.65, respectively, in Fig. 7. For the case of $\chi = 0$, it describes a merger of two nonrotating black holes. If these two black holes have the same mass parameter $\nu = 0.25$, then we will obtain $a_f \approx 0.6631$ for the Kerr black hole with $\alpha = 0$. Interestingly, this value will decrease when α is nonvanishing. For example, $a_f \approx 0.6368$, 0.6160, 0.5990, 0.5847, 0.5724 for $\alpha = 0.2$, 0.4, 0.6, 0.8, 1, respectively. We can also find that the final spin a_f increases with ν, while it decreases with α. If these black holes have initial spins, the results are similar [see Figs. 7(b)–7(d)].

On the other hand, we would like to examine the behavior of the final spin a_f when the two merged black holes approach its extremal case. For this purpose, we list the final spin a_f for $\chi = 0.99\frac{1}{\sqrt{1+\alpha}}$ in Fig. 8. From it, one can clearly see that the final spin decreases with the mass parameter ν, which is quite different from that of Fig. 7. This is a novel result. And it is also consistent with the result given in Refs. [27,28].

Next, we consider another simple case that the two initial black holes have the same mass, i.e., $\nu = 0.25$. Then we present the final spin a_f for different initial values of the spin χ in Fig. 9. Positive or negative χ denotes that the initial spin is either aligned or antialigned with respect to the initial orbital angular momentum. From the figure, it is clear that the final spin a_f increases with χ from negative to positive values. For fixed χ, the final spin a_f decreases with α. For example, varying $\alpha = 0$, 0.2, 0.4, 0.6, 0.8, 1, $a_f(\chi = -0.5)/M \approx 0.4819$, 0.4599, 0.4430, 0.4296, 0.4186, 0.4094 and $a_f(\chi = 0.5)/M \approx 0.8281$, 0.7935, 0.7645, 0.7391, 0.7158, 0.6936. Moreover, we can also obtain the result that no matter the initial spin's

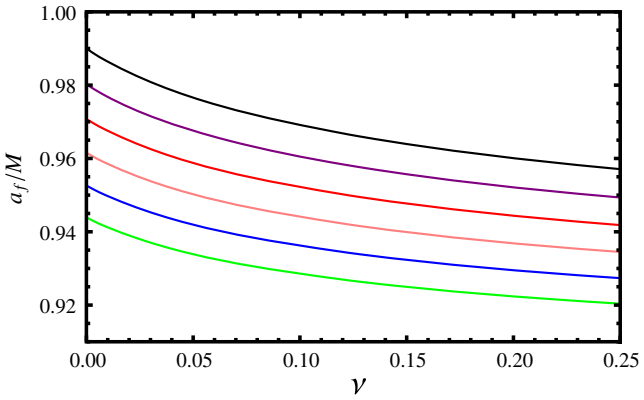

FIG. 8. Final spin a_f vs mass parameter ν for equal spin merger with initial high spin $\chi = 0.99\,\frac{1}{\sqrt{1+\alpha}}$. The parameter $\alpha = 0$, 0.02, 0.04, 0.06, 0.08, 0.1 from top to bottom.

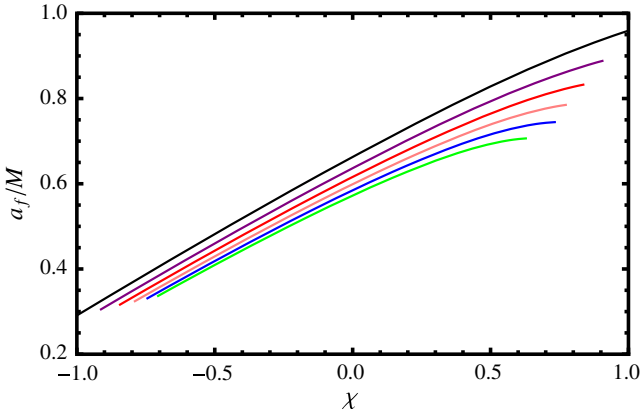

FIG. 9. Final spin a_f vs initial spin χ for equal spin and equal mass black hole merger with $\alpha = 0$, 0.2, 0.4, 0.6, 0.8, 1 from top to bottom.

alignment or antialignment, the final spin of the black hole is always aligned with the initial orbital angular momentum.

D. Unequal spin merger

In this subsection, we would like to consider the unequal spin case but with equal mass. So we set $\chi_2 = \beta\chi$, $\chi_1 = \chi$, and $\nu = 0.25$. Adopting these values, the final spin will be in the following form:

$$a_f = \frac{1}{4}(L(r_{\rm ISCO}, a_f) + M\chi + \beta M\chi). \tag{48}$$

Taking one of the black hole spins as 0.5, and regarding that it is aligned or antialigned with respect to the initial orbital angular momentum, we illustrate the value of the final spin parameter for equal mass black holes in Fig. 10. Because β varies from -1 to 1, we can see that the final spin increases or decreases with β for an aligned or an antialigned case. It is also obvious that the final spin decreases with α for both cases.

E. Generic spin configuration merger

Now, we consider a generic spin configuration merger, which means that the orbit plane of the ISCO can be inclined with respect to the final total angular momentum. For this case, the calculation of the orbital contribution to the total angular momentum is required to perform a numerical integration of generic geodesics in the black hole background or use the radial potential for some certain quasiadiabatic spherical orbits [37]. On the other hand, one can alternatively adopt the fit formula given in Ref. [38]. Here we choose the latter one. Then the orbital angular momentum of the inclined orbit reads [27,38]

$$L(\vartheta, a_f) = \frac{1}{2}(1+\cos\vartheta)L^{\rm pro}(r^{\rm pro}_{\rm ISCO}, a_f) + \frac{1}{2}(1-\cos\vartheta)|L^{\rm ret}(r^{\rm ret}_{\rm ISCO}, a_f)|, \tag{49}$$

where the inclination angle ϑ measures the angle between the final spin a_f and the orbital angular momentum. Let us

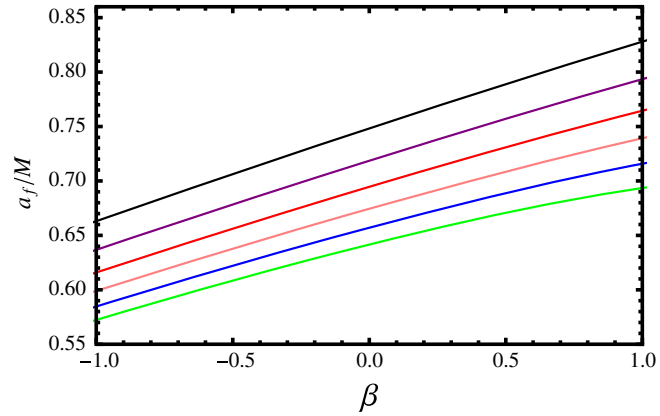

(a)

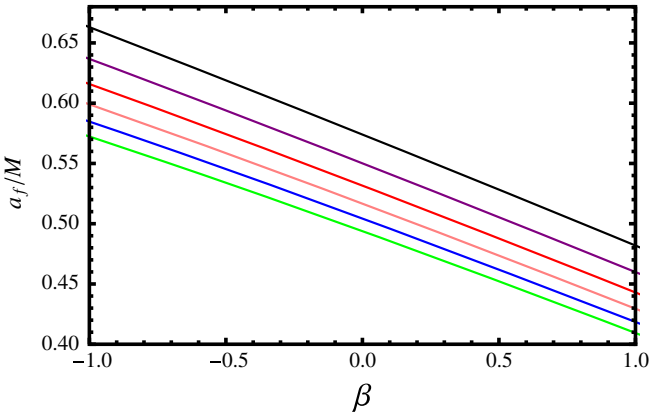

(b)

FIG. 10. Final spin a_f vs β for unequal spin merger with $\alpha = 0$, 0.2, 0.4, 0.6, 0.8, 1 from top to bottom. (a) $\chi = 0.5$. (b) $\chi = -0.5$.

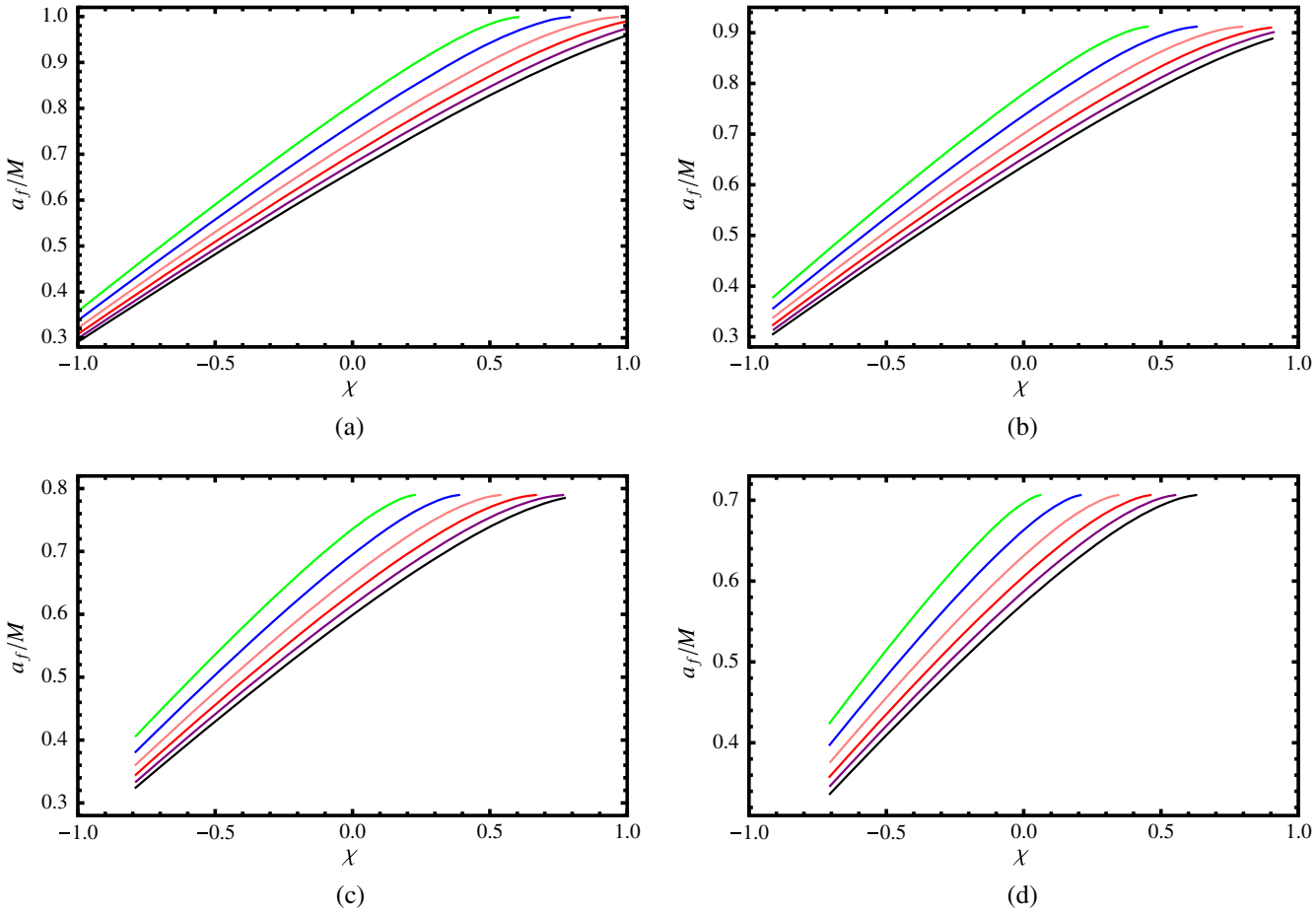

FIG. 11. Final spin a_f vs χ with $\vartheta = 0°, 30°, 45°, 60°, 75°, 90°$ from bottom to top. (a) $\alpha = 0$. (b) $\alpha = 0.2$. (c) $\alpha = 0.6$. (d) $\alpha = 1$. Note that $|\chi| \leq \frac{1}{\sqrt{1+\alpha}}$ for a black hole merger.

consider a simple case where these two merged black holes have the same masses and spins. Thus the final spin a_f can be solved as

$$a_f = \frac{1}{8}(L^{\text{pro}} + |L^{\text{ret}}| + 4M\chi + (L^{\text{pro}} - |L^{\text{ret}}|)\cos\vartheta). \quad (50)$$

Here we show the final spin a_f as a function of χ for different values of ϑ and α in Fig. 11. From it, we can see that the angle ϑ has a significant influence on the final spin a_f. And with the increase of ϑ, the final spin a_f increases.

V. CONCLUSIONS

In this paper, we studied the main features of the Kerr-MOG black hole merger in a modified gravity. The results show a significant dependence on the dimensionless scalar field parameter α.

At first, we explored the property and geodesics for the Kerr-MOG black hole. For the nonrotating case with $\alpha \neq 0$, the black hole has two horizons, which is different from the Schwarzschild black hole case. On the other hand, compared to the rotating Kerr black hole, the maximum spin will be reduced by α, i.e., $a_{\max}/M = \frac{1}{\sqrt{1+\alpha}}$. Then the geodesics was obtained, which also shows an α-dependent property.

Based on the null geodesics, we investigated the gravitational waves at the ringdown stage, which can be effectively approximated by the light rings. The real and imaginary parts are, respectively, described by the angular velocity Ω_c and the Lyapunov exponent λ. Our result implies that, for the prograde orbit, Ω_c increases with α, and λ increases with α for small a while it decreases with α for large a. For the retrograde orbit, Ω_c decreases with α, while λ increases with it.

Next, using the result of the ISCO for the massive particles, we estimated the final black hole spin via the BKL recipe. Several especially interesting cases were explored.

For the case of the equal spin merger, the final spin a_f decreases with the dimensionless scalar field parameter α. It was also found that the final spin a_f increases with ν for a low initial spin. While the initial spin approaches its maximum value, a_f will not increase but will decrease with ν; see Fig. 8. So we can expect that there may exist a critical value of χ where the final spin a_f is independent of the

mass parameter ν. Certainly, such a critical value will be reduced by α. Further, if these two merged black holes have equal masses, the final spin will also be reduced by α. Nevertheless, no matter the initial spin's alignment or antialignment, the final spin of the black hole is always aligned with the initial orbital angular momentum.

For the case of the unequal spin merger, we found that the final spin increases or decreases with β for an aligned or an antialigned case. Moreover, for both the cases, the final spin presents a monotonically decreasing behavior with the increase of the dimensionless scalar field parameter α.

We also considered the generic spin configuration merger, which allows that the orbit plane has an inclination angle with respect to the final total angular momentum. Then we adopted the fit formula given in Ref. [38] to modify the orbital angular momentum. Considering the two black holes have equal mass and spin, we studied the final spin a_f as the initial spin χ for different inclination angles ϑ and α. The result implies that the final spin a_f increases with the inclination angle ϑ.

In summary, our study reveals that for this modified gravity, the black hole merger closely depends on its characteristic parameter, i.e., the dimensionless scalar field parameter α. We expected that such an influence of α can be determined by the gravitational wave detection in the near future.

ACKNOWLEDGMENTS

This work was supported by the National Natural Science Foundation of China (Grants No. 11675064, No. 11522541, No. 11375075, and No. 11205074).

[1] B. P. Abbott *et al.* (Virgo and LIGO Scientific Collaborations), Observation of Gravitational Waves from a Binary Black Hole Merger, Phys. Rev. Lett. **116**, 061102 (2016); GW151226: Observation of Gravitational Waves from a 22-Solar-Mass Binary Black Hole Coalescence, Phys. Rev. Lett. **116**, 241103 (2016); B. Abbott *et al.* (VIRGO and LIGO Scientific Collaborations), GW170104: Observation of a 50-Solar-Mass Binary Black Hole Coalescence at Redshift 0.2, Phys. Rev. Lett. **118**, 221101 (2017); GW170814: A Three-Detector Observation of Gravitational Waves from a Binary Black Hole Coalescence, Phys. Rev. Lett. **119**, 141101 (2017); GW170817: Observation of Gravitational Waves from a Binary Neutron Star Inspiral, Phys. Rev. Lett. **119**, 161101 (2017); GW170608: Observation of a 19-Solar-Mass Binary Black Hole Coalescence, Astrophys. J. **851**, L35 (2017).

[2] R. Konoplya and A. Zhidenko, Detection of gravitational waves from black holes: Is there a window for alternative theories?, Phys. Lett. B **756**, 350 (2016).

[3] A. Cardenas-Avendano, J. Jiang, and C. Bambi, Testing the Kerr black hole hypothesis: Comparison between the gravitational wave and the iron line approaches, Phys. Lett. B **760**, 254 (2016).

[4] M. M. Caldarelli, G. Cognola, and D. Klemm, Tests of General Relativity with GW150914, Phys. Rev. Lett. **116**, 221101 (2016).

[5] N. Yunes, K. Yagi, and F. Pretorius, Theoretical physics implications of the binary black-hole mergers GW150914 and GW151226, Phys. Rev. D **94**, 084002 (2016).

[6] J. W. Moffat, Scalar-tensor-vector gravity theory, J. Cosmol. Astropart. Phys. 03 (2006) 004.

[7] J. W. Moffat and S. Rahvar, The MOG weak field approximation and observational test of galaxy rotation curves, Mon. Not. R. Astron. Soc. **436**, 1439 (2013).

[8] J. W. Moffat and S. Rahvar, The MOG weak field approximation. II. Observational test of Chandra X-ray clusters, Mon. Not. R. Astron. Soc. **441**, 3724 (2014).

[9] J. W. Moffat and V. T. Toth, Rotational velocity curves in the Milky Way as a test of modified gravity, Phys. Rev. D **91**, 043004 (2015).

[10] J. W. Moffat, Black holes in modified gravity (MOG), Eur. Phys. J. C **75**, 175 (2015).

[11] J. W. Moffat, Modified gravity black holes and their observable shadows, Eur. Phys. J. C **75**, 130 (2015).

[12] J. R. Mureika, J. W. Moffat, and M. Faizal, Black hole thermodynamics in modified gravity (MOG), Phys. Lett. B **757**, 528 (2016).

[13] H.-C. Lee and Y.-J. Han, Inner-most stable circular orbit in Kerr-MOG black hole, Eur. Phys. J. C **77**, 655 (2017).

[14] M. Sharif and M. Shahzadi, Particle dynamics near Kerr-MOG black hole, Eur. Phys. J. C **77**, 363 (2017).

[15] S. Hussain and M. Jamil, Timelike geodesics of a modified gravity black hole immersed in an axially symmetric magnetic field, Phys. Rev. D **92**, 043008 (2015).

[16] D. Perez, F. G. L. Armengol, and G. E. Romero, Accretion disks around black holes in scalar-tensor-vector gravity, Phys. Rev. D **95**, 104047 (2017).

[17] P. Sheoran, A. Herrera-Aguilar, and U. Nucamendi, Mass and spin of a Kerr-MOG black hole and a test for the Kerr black hole hypothesis, Phys. Rev. D **97**, 124049 (2018).

[18] J. W. Moffat, Misaligned spin merging black holes in modified gravity (MOG), arXiv:1706.05035.

[19] L. Manfredi, J. Mureika, and J. Moffat, Quasinormal modes of modified gravity (MOG) black holes, Phys. Lett. B **779**, 492 (2018).

[20] V. Cardoso, A. S. Miranda, E. Berti, H. Witek, and V. T. Zanchin, Geodesic stability, Lyapunov exponents and quasinormal modes, Phys. Rev. D **79**, 064016 (2009).

[21] K. Glampedakis, G. Pappas, H. O. Silva, and E. Berti, Post-Kerr black hole spectroscopy, Phys. Rev. D **96**, 064054 (2017).
[22] E. Berti and K. D. Kokkotas, Quasinormal modes of Kerr-Newman black holes: Coupling of electromagnetic and gravitational perturbations, Phys. Rev. D **71**, 124008 (2005).
[23] G. Khanna and R. H. Price, Black hole ringing, quasinormal modes, and light rings, Phys. Rev. D **95**, 081501 (2017).
[24] R. A. Konoplya and Z. Stuchlik, Are eikonal quasinormal modes linked to the unstable circular null geodesics?, Phys. Lett. B **771**, 597 (2017).
[25] J. L. Blázquez-Salcedo, C. F. B. Macedo, V. Cardoso, V. Ferrari, L. Gualtieri, F. S. Khoo, J. Kunz, and P. Pani, Perturbed black holes in Einstein-dilaton-Gauss-Bonnet gravity: Stability, ringdown, and gravitational-wave emission, Phys. Rev. D **94**, 104024 (2016).
[26] J. L. Blázquez-Salcedo, F. S. Khoo, and J. Kunz, Quasinormal modes of Einstein-Gauss-Bonnet-dilaton black holes, Phys. Rev. D **96**, 064008 (2017).
[27] A. Buonanno, L. E. Kidder, and L. Lehner, Estimating the final spin of a binary black hole coalescence, Phys. Rev. D **77**, 026004 (2008).
[28] P. Jai-akson, A. Chatrabhuti, O. Evnin, and L. Lehner, Back hole merger estimates in Einstein-Maxwell and Einstein-Maxwell-dilaton gravity, Phys. Rev. D **96**, 044031 (2017).
[29] M. Kesden, Can binary mergers produce maximally spinning black holes?, Phys. Rev. D **78**, 084030 (2008).
[30] B. Mashhoon, *Proceedings of the Third Marcel Grossmann Meeting on Recent Developments of General Relativity, Shanghai, 1982*, edited by Hu Ning (North-Holland, Amsterdam, 1983).
[31] B. F. Schutz and C. M. Will, Black hole normal modes: A semianalytic approach, Astrophys. J. **291**, L33 (1985).
[32] S. Iyer and C. M. Will, Black-hole normal modes: A WKB approach. I. Foundations and application of a higher-order WKB analysis of potential-barrier scattering, Phys. Rev. D **35**, 3621 (1987).
[33] E. Berti, V. Cardoso, T. Hinderer, M. Lemos, F. Pretorius, U. Sperhake, and N. Yunes, Semianalytical estimates of scattering thresholds and gravitational radiation in ultrarelativistic black hole encounters, Phys. Rev. D **81**, 104048 (2010).
[34] U. Sperhake, V. Cardoso, C. D. Ott, E. Schnetter, and H. Witek, Collisions of unequal mass black holes and the point particle limit, Phys. Rev. D **84**, 084038 (2011).
[35] A. Le Tiec, The overlap of numerical relativity, perturbation theory and post-Newtonian theory in the binary black hole problem, Int. J. Mod. Phys. D **23**, 1430022 (2014).
[36] J. Bardeen, W. H. Press, and S. Teukolsky, Rotating black holes locally nonrotating frames, energy extraction, and scalar synchrotron radiation, Astrophys. J. **178**, 347 (1972).
[37] S. Chandrasekhar, *The Mathematical Theory of Black Holes* (Clarendon Press, Oxford, 1998).
[38] S. A. Hughes and R. D. Blandford, Black hole mass and spin coevolution by mergers, Astrophys. J. **585**, L101 (2003).